Supplemental Materials: Franck-Condon tuning of optical cycling centers by organic functionalization

EFFECTS CONSIDERED IN FRANCK-CONDON CALCULATIONS

Since the accuracy of TD-DFT and DFT for calculating FCFs is not well established, we first benchmark our methods on small molecules for which experimental measurements (as well as higher levels of theory) are available, finding that our methods agree to better than 2%. We then investigated additional effects that could be considered in polyatomic molecules, and estimated the magnitude of the change in vibrational branching that could be induced by perturbations. In light of our benchmark, those that are smaller than 2% are considered negligible compared to the systematic uncertainty. Further, we justify that by design, these molecular FCFs are well-described by the harmonic parallel approximation in a single reference formalism.

Method

Our TD-DFT and DFT methods used for MOC_6H_5 calculations (with Gaussian16 [1]) were benchmarked on M-OH molecules with higher levels of theory, specifically state-averaged CASSCF to optimize geometries, and the MRCI method to calculate electronic excitation energies with Molpro [2]-[3]. We then estimated the error in the FCF double-harmonic approximation (obtained with ezSpectrum [4]) through benchmarked bond length changes compared to experiment. All molecules and molecular orbitals were generated using Multiwfn [5].

We chose MOH molecules based on available experimental data and size: our MOC_6H_5 molecules are too large to perform full CASSCF/MRCI. For MOH, SA-CASSCF geometry optimizations were performed with an active space of 9 electrons and 10 orbitals. The calculations were averaged over the ground and doubly degenerate excited state with a weight of 0.8/0.1/0.1 for the ground state and 0.2/0.4/0.4 for the excited state. The MRCI method, with three reference states, was then used to compute the vertical excitation energies.

In Table S-i we compare the geometries and excitation energies of M-OH and M-OCH_3 systems between DFT, MRCI/CASSCF, and experimental values (where available). Since MOC_6H_5 is similar in structure to M-OH and $MOCH_3$, and has the same dominant modes involved in FCFs (the M-O stretch), we tentatively use this DFT theory to describe our larger system, and focus on relative trends of the substituent effect on FCF under this theory.

Molecule	Method	FCF	$X^2\Sigma^+$ M-O (Å)	$A^2\Pi$ M-O (Å)	M-O change (Å)	E_{ex} (eV)
CaOH	TD-DFT	0.934	1.974	1.950	-0.025	1.973
	CASSCF/MRCI		2.030	1.999	-0.030	
	Experiment [6–8]	0.9539(21)	1.975	1.953	-0.021	1.979, 1.988
SrOH	TD-DFT	0.945	2.095	2.073	-0.022	1.737
	CASSCF/MRCI		2.145	2.117	-0.028	
	Experiment [8–10]	0.958(3)	2.111	2.091	-0.020	1.803, 1.836
$CaOCH_3$	TD-DFT	0.937	1.973	1.951	-0.022	1.901
	Experiment [11]	0.925(7)				
$SrOCH_3$	TD-DFT	0.923	2.095	2.073	-0.022	1.740

TABLE S-i. Comparison between different computational methods for the M-O (M = Ca, Sr) bond lengths (in Å) of alkaline earth oxide species in the $\tilde{X}$ and $\tilde{A}$ states, as well as the bond length changes from $\tilde{X}$ to $\tilde{A}$, and the vertical excitation energy (E_{ex} in eV), compared to the band origins or measured FCFs from experiment.

Functional and Basis Set

We found the PBE0 hybrid functional [12] with the D3 dispersion correction [13] yielded the most reliable DFT and excited state calculations (Table S-ii), which is well known [14–21]. We also probed the effects of basis set size

and functional (Table S-ii). Based on overall best performance, DFT geometry optimizations and energy excitations for this work were computed with the PBE0-D3/def2-TZVPPD [22] level of theory on a superfine grid with very tight convergence parameters in Gaussian16. The def2 effective core potential (ECP) was used for the Sr atom.

Functional	Basis Set	$X^2\Sigma^+$ Sr-O (Å)	$A^2\Pi$ Sr-O (Å)	Sr-O change (Å)	E_{ex} (eV)
B3LYP-D3	def2-TZVPPD	2.115	2.096	-0.019	1.896
m062x	def2-TZVPPD	2.108	2.102	-0.006	2.228
ωB97XD	def2-TZVPPD	2.113	2.087	-0.026	1.668
PBE0-D3	def2-TZVPPD	2.095	2.073	-0.022	1.737
PBE0-D3	def2-SVPD/def2-TZVPPD	2.138	2.121	-0.017	1.750
Experiment [8, 10]		2.111	2.091	-0.020	1.803, 1.836

TABLE S-ii. Comparison between different basis sets and TD-DFT functionals for calculating the Sr-O bond lengths (in Å) of SrOH and $A^2\Pi$ states, the bond length changes from $X^2\Sigma^+$ to $A^2\Pi$, and the vertical excitation energy (E_{ex} in eV). Results are compared to band origins from experiment.

To estimate potential error in FCFs, we briefly discuss the double-harmonic approximation calculated with ezSpectrum. Previous studies estimate that double-harmonic approximation FCFs have 2-3% error with equilibrium bond length values that differed from experimental values by 0.001 – 0.03 Angstroms and computed bond length change from $\tilde{X}$ to $\tilde{A}$ agreed with experiment within 0.003-0.006 Angstroms [23]. Similarly, our current method of PBE0-D3 with def2-TZVPPD basis set and ECP gave bond length values for SrOH and CaOH within 0.001 Angstroms of experiment and 0.004 Angstroms for bond length change (Table S-i). Additionally, FCFs using a higher level single-reference method, CCSD/EOM-CCSD, have been previously reported [24] for $\tilde{A} \rightarrow \tilde{X}$ in $CaOC_6H_5$ as $q_{0,0} = 0.8329$. However, we found the TD-DFT bond lengths on both the ground, and the excited states of $CaOC_6H_5$, and bond length differences from $\tilde{X} \rightarrow \tilde{A}$, are nearly identical to those computed with EOM-CCSDT and reported in [24]. More detailed investigations into FCF errors, specifically for our MOC_6H_5 molecules, are discussed in the following sections.

Duschinsky Rotations

Duschinsky rotations can be used to change coordinates between states when the normal modes between the excited and ground state are sufficiently non-parallel. However, for our systems, the normal modes between the ground and excited states are quite parallel. This is by design, as the largest geometry change in our molecules are the Ca-O/Sr-O stretch bond length, and the dominant off-diagonal Franck-Condons are associated with this stretching motion. As such, this behavior, and the change in stretch behavior as withdrawing groups are added, is seen equally by both the ground and excited state and there is no other significant change in geometry or mode motion. For this reason, the parallel approximation holds as a way to calculate Franck-Condon factors for these molecules.

To test this approximation, selected FCFs were also calculated using Duschinsky rotations and reported in Table S-iii. Only a small change in FCF ($< 10^{-3}$) was found between Duschinsky rotations and the parallel approximation using harmonic vibrational frequencies, with the same FCF improvement from $CaOC_2H_5$ to $CaOC_9H_2F_9$. Gaussian16 [1] was used to calculate FCFs with Duschinsky rotations and ezSpectrum [4] was used to calculate FCFs with the parallel approximation. The magnitude (and sign) of the small correction here is similar for both the unsubstituted and maximally-substituted variants of calcium phenoxide, suggesting that substitution does not introduce additional problematic Duschinsky effects.

Molecule	FCF, parallel approximation	FCF, Duschinsky rotations
$CaOC_2H_5$	0.9575	0.9573
$CaOC_9H_2F_9$	0.9981	0.9976

TABLE S-iii. Calculated FCFs for $CaOC_2H_5$ and $CaOC_2H_5$ in the parallel approximation and with Duschinsky rotations.

Anharmonicity

For the molecules studied, the largest geometry change upon excitation is the M-O bond length, and the dominant off-diagonal FCFs are associated with this motion. Since we are primarily concerned with the features of the two potentials near their minima (as we are interested in vibrational ground states), the harmonic approximation is expected to hold, particularly for the deep M-O stretch modes.

To test this, we calculated the cubic and quartic contributions to the potentials, and constructed a one-mode model for the M-O stretch mode for three species. We find that for calcium phenoxide in the unsubstituted, meta-CF_3 substituted, and 3,4,5-F substituted variants, the dominant perturbations (cubic) for the ground state match those for the excited state to better than 10%, with the excitate state perturbation slightly stronger than the ground state. Since this relaxes the excited well toward the ground well's equilibrium position, this improved the FCFs for all three species, though by only a very small amount (less than 0.3%).

Vibrational Branching Ratio

The $\tilde{\mathrm{A}} \leftrightarrow \tilde{\mathrm{X}}$ transition for calcium phenoxide is expected to be centered spectroscopically near 600 nm $< \lambda <$ 650 nm. Using this, the vibrational branching ratio (VBR) was calculated by weighting each FCF by the cube of its transition frequency and normalizing. The VBR calculated in this way was less than 0.6% larger than the FCF. Further, this correction would not be expected to change scale with substitution.

Nonadiabatic vibronic coupling

A number of recent, high-precision measurements of vibrational branching ratios for laser-coolable MOR molecules have found that interactions among the electronically excited states can introduce additional off-diagonal decays. This intensity borrowing can arise from a number of interactions, including the Renner-Teller [6], spin-orbit-vibronic [25], Fermi resonance [6], and Jahn-Teller effects [26, 27]. Quite generally, such perturbations are more likely when a molecule has low symmetry, low vibrational frequencies, and a large number of normal modes. Different experimental goals will require different photon budgets; these may range from ∼100 photons for high-fidelity imaging, to ∼1000 photons for transverse sub-Doppler laser cooling, to $> 10^4$ photons for full 3D cooling and trapping [28]. Because cycling $\sim 10^2 - 10^3$ photons without significant loss of population requires vibrational closure at the level of 10^{-3}, any mixings above this level must be understood and mitigated for optical detection and transverse cooling applications. Experiments aimed at producing laser-cooled and trapped molecules, by contrast, must control all losses at the $< 10^{-4}$ level.

While a full characterization of these vibronic coupling effects requires an intensive study of the potential energy surfaces for each molecule of interest [27, 29–31], we can gain general insight by using well-developed perturbation methods [6, 32–34]. Consider, for example, the case of $SrOC_9H_2F_9$. Starting from the computed vibrational frequencies and electronic excitation energies, we identified all possible near-degeneracies (defined as levels within 15 cm^{-1} of one another) among the $\tilde{\mathrm{A}}$, $\tilde{\mathrm{B}}$, and $\tilde{\mathrm{C}}$ states. Nearly two dozen near-degeneracies were found. Using the linear vibronic coupling matrix elements inferred from or calculated by previous works [26, 27], we find that both the $\tilde{\mathrm{B}}(v = 0)$ state is perturbed by the vibrationally excited levels of $\tilde{\mathrm{A}}$ so as to exhibit $\gtrsim 1\%$ of emission into excited bending modes in $\tilde{\mathrm{X}}$. A similar situation is found for $\tilde{\mathrm{C}}$, although in this case perturbations from excited vibrations of both $\tilde{\mathrm{A}}$ and $\tilde{\mathrm{B}}$ contribute to the intensity borrowing effect. Because these effects are larger than the decays expected based on calculations for which the (unperturbed) vibrational modes are taken as eigenstates, the utility of the $\tilde{\mathrm{B}}$ or $\tilde{\mathrm{C}}$ states for optical cycling will require careful experimental study of vibrational loss channels are opened up by vibronic interaction.

The situation for the $\tilde{\mathrm{A}}(v = 0)$ state is different because there are no near-degenerate electronic states below it, and therefore no accidental near degeneracies. However, previously, second-order effects operating within the $\tilde{\mathrm{A}}$ manifold were found to induce losses to then-unexpected vibrational bending modes [6, 25–27, 35]. Based on the previous measurements of these effects, and scaling for the energy splittings in the molecules considered in this paper, we predict such loss channels to be active only at a level smaller than 10^{-3}. Such a value is sufficiently low that it will not impact the efficiency of photon cycling considered in the main text. In order to extend photon cycling to $\gg 100$ photons, it will be important to reconsider these small couplings. Based on this analysis, the $\tilde{\mathrm{A}}(v = 0)$ states of the (possibly substituted) calcium and strontium phenoxides appears to be the best choice for efficient photon cycling in

future experiments. Depending on the degree of vibrational closure required, the $\tilde{B}$ and $\tilde{C}$ states could still be used for higher-order vibrational repumping without sacrificing much population.

Dissociative decay

The lowest energy dissociated state for these molecular derivatives was calculated to lie above the $\tilde{X} \rightarrow \tilde{A}$ electronic transition by 6-7 eV. As such, the optical excitation energy for the first excited state is not enough to dissociate the molecule.

NATURAL TRANSITION ORBITALS

Calculated natural transition orbitals (NTO) are shown in Figure S1 for the first electronic excitation of $SrOC_6H_5$ and Figure S2 for the first four electronic excitations of substituted alkaline earth phenoxides. NTOs provide a better description of excited state electron density than molecular orbitals in particle-hole excitations. Transforming molecular orbital electron density to natural transition orbital density involves separate unitary transformations on both occupied and unoccupied orbitals to obtain a localized transition density matrix to describe the electronic transition [36, 37]. Figure S2 shows that substituting 4-NO_2 for a hydrogen on $SrOC_6H_5$ reorders the excited states to favor mixing electron density on the NO_2 and the metal, so the transition is less localized. As such, it produces a poorer FCF ($\tilde{A} \rightarrow \tilde{X}$ $q_{0,0} = 0.8017$) despite electron-withdrawing strength. This is because NO_2 promotes delocalization through the π system of its molecular orbitals with the benzene ring.

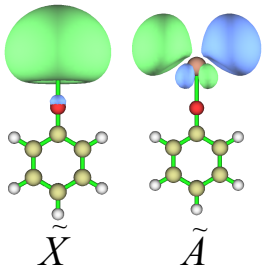

Figure S1. Natural transition orbitals for $SrOC_6H_5$'s $\tilde{X} \rightarrow \tilde{A}$ electronic transition. Orbitals were generated using an isosurface value of 0.03.

HAMMETT PARAMETERS

Hammett parameters quantify substituents' electron-withdrawing strengths at particular sites on the phenyl ring. These parameters are empirically derived constants based on ionizing benzoic acid in water at room temperature. Although Hammett parameters can be generalized to other systems, we use the original σ_m and σ_p definitions which involve ionizing benzoic acid with substituents in meta or para positions, tabulated in Table 1 of Hansch *et al.* [38]. Benzoic acid is similar in structure to our alkaline earth phenoxides, so these Hammett parameters are reliable in predicting electron-withdrawing strengths for this system. Electron-withdrawing groups have positive Hammett parameters, while electron donating groups have negative Hammett parameters (the unsubstituted case, $SrOC_6H_5$, has a Hammett parameter of 0). Ref. [38] lists Hammett constants for the substituents we considered, which range from $\sigma_{\text{tot}} = -0.37$ for the electron-donating para-OH substitution to $\sigma_{\text{tot}} = 1.40$ for phenyl decorated with three strongly electron-withdrawing CF_3 groups. With multiple substituents, individual Hammett parameters were added to approximate the net effect.

Trends with Hammett total

Figure S3 shows the approximately linear dependence of the bond length change upon de-excitation on the Hammett total of the substituents. The x-intercepts represent the Hammett totals for which the bond length would not change

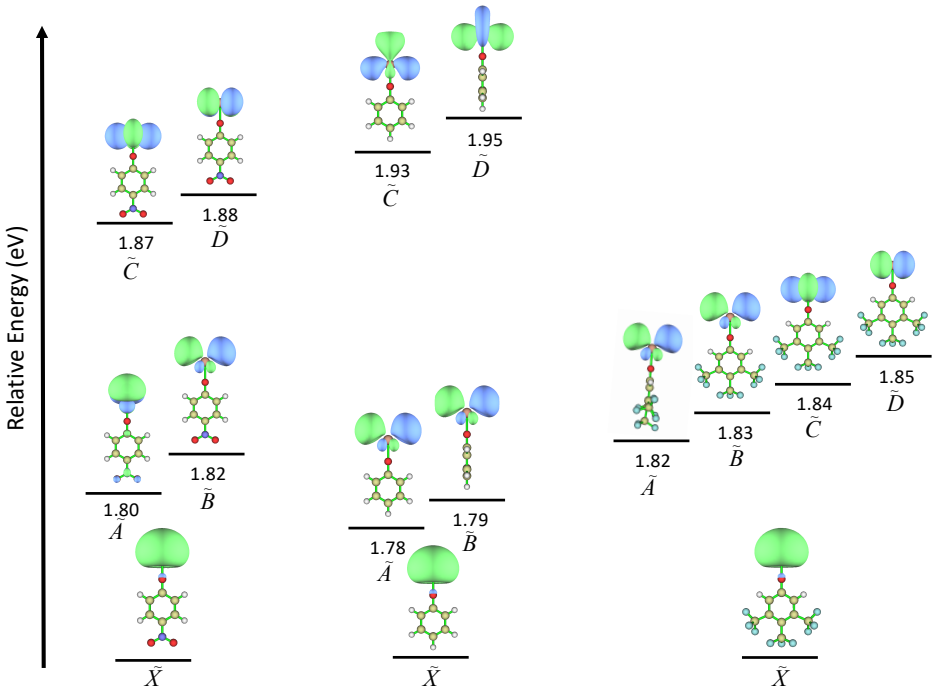

Figure S2. Natural transition orbitals for $\tilde{A} \rightarrow \tilde{X}$, $\tilde{B} \rightarrow \tilde{X}$, $\tilde{C} \rightarrow \tilde{X}$ and $\tilde{D} \rightarrow \tilde{X}$ transitions for $SrOC_9H_2F_9$, $SrOC_6H_5$ and SrO_3C_6HN. Orbitals were generated using an isosurface value of 0.03.

upon excitation (should such a total be achievable in a way that does not violate the stipulations described in the main text).

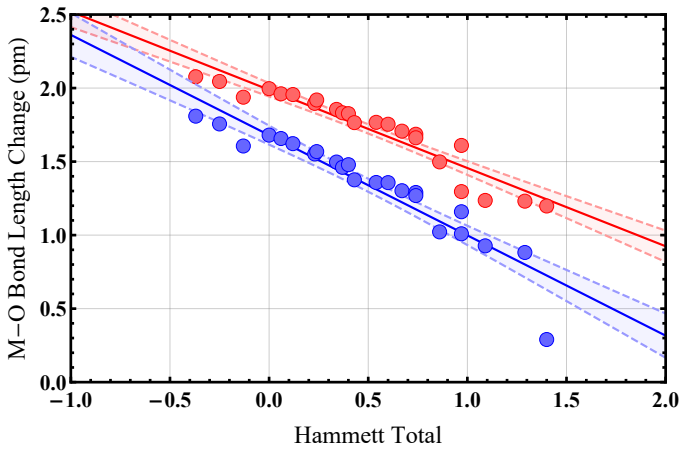

Figure S3. The amount by which the M-O bond length changes upon $\tilde{A} \rightarrow \tilde{X}$ is strongly dependent on the Hammett total of any substituents. Linear fits for the Sr- species (red) and Ca- species (blue) have x-intercepts at $\Sigma\sigma = 3.7$ and 2.5, respectively. Colored bands here and in Fig. 2 of the main text represent 90% confidence intervals for the fits.

The curves fit to the FCF vs. Hammett total calculations in Fig. 2 of the main text are Gaussians centered on the x-intercepts of the fit lines in Fig. S3 (denoted by $\bar{x}$). The free parameters a and w were fit using

$$q_{0,0}(x) = a\mathrm{e}^{-(x-\bar{x})^2/w^2} \tag{S1}$$

with x the Hammet total. Fitted parameters were $a = 0.998(4)$ and $w = 14.0(5)$ for Sr species and $a = 0.996(2)$ and $w = 12.2(4)$ for Ca species.

[1] M. J. Frisch, G. W. Trucks, H. B. Schlegel, G. E. Scuseria, M. A. Robb, J. R. Cheeseman, G. Scalmani, V. Barone, G. A. Petersson, H. Nakatsuji, X. Li, M. Caricato, A. V. Marenich, J. Bloino, B. G. Janesko, R. Gomperts, B. Mennucci, H. P. Hratchian, J. V. Ortiz, A. F. Izmaylov, J. L. Sonnenberg, D. Williams-Young, F. Ding, F. Lipparini, F. Egidi, J. Goings, B. Peng, A. Petrone, T. Henderson, D. Ranasinghe, V. G. Zakrzewski, J. Gao, N. Rega, G. Zheng, W. Liang, M. Hada, M. Ehara, K. Toyota, R. Fukuda, J. Hasegawa, M. Ishida, T. Nakajima, Y. Honda, O. Kitao, H. Nakai, T. Vreven, K. Throssell, J. A. Montgomery, Jr., J. E. Peralta, F. Ogliaro, M. J. Bearpark, J. J. Heyd, E. N. Brothers, K. N. Kudin, V. N. Staroverov, T. A. Keith, R. Kobayashi, J. Normand, K. Raghavachari, A. P. Rendell, J. C. Burant, S. S. Iyengar, J. Tomasi, M. Cossi, J. M. Millam, M. Klene, C. Adamo, R. Cammi, J. W. Ochterski, R. L. Martin, K. Morokuma, O. Farkas, J. B. Foresman, and D. J. Fox, "Gaussian˜16 Revision C.01," (2016), gaussian Inc. Wallingford CT.

[2] H.J. Werner, P.J. Knowles, G. Knizia, F.R. Manby, and M. Schütz, Wiley Interdiscip. Rev. Comput. Mol. Sci. **2**, 242–253 (2012).

[3] H.-J. Werner, P. J. Knowles, G. Knizia, F. R. Manby, M. Schütz, P. Celani, W. Györffy, D. Kats, T. Korona, R. Lindh, A. Mitrushenkov, G. Rauhut, K. R. Shamasundar, T. B. Adler, R. D. Amos, S. J. Bennie, A. Bernhardsson, A. Berning, D. L. Cooper, M. J. O. Deegan, A. J. Dobbyn, F. Eckert, E. Goll, C. Hampel, A. Hesselmann, G. Hetzer, T. Hrenar, G. Jansen, C. Köppl, S. J. R. Lee, Y. Liu, A. W. Lloyd, Q. Ma, R. A. Mata, A. J. May, S. J. McNicholas, W. Meyer, T. F. Miller III, M. E. Mura, A. Nicklass, D. P. O'Neill, P. Palmieri, D. Peng, K. Pflüger, R. Pitzer, M. Reiher, T. Shiozaki, H. Stoll, A. J. Stone, R. Tarroni, T. Thorsteinsson, M. Wang, and M. Welborn, "Molpro, version 2019.2, a package of *ab initio* programs," (2019), see https://www.molpro.net.

[4] V.A. Mozhayskiy and A.I. Krylov, "ezSpectrum," http://iopenshell.usc.edu/downloads.

[5] F. Lu, T.; Chen, "Multiwfn: A multifunctional wavefunction analyzer." J. Comput. Chem. **33**, 580–592 (2012).

[6] L. Baum, N. B. Vilas, C. Hallas, B. L. Augenbraun, S. Raval, D. Mitra, and J. M. Doyle, "Establishing a highly closed cycling transition in a polyatomic molecule," (2020), arXiv:2006.01769.

[7] M. Li and J.A. Coxon, J. Chem. Phys. **104**, 4961–4977 (1996).

[8] C.R. Brazier, L.C. Ellingboe, S. Kinsey-Nielsen, and P.F. Bernath, J. Am. Chem. Soc. **108**, 2126–2132 (1986).

[9] Duc-Trung Nguyen, Timothy C. Steimle, Ivan Kozyryev, Meng Huang, and Anne B. McCoy, "Fluorescence branching ratios and magnetic tuning of the visible spectrum of SrOH," Journal of Molecular Spectroscopy **347**, 7–18 (2018).

[10] S. Yu, J.G. Wang, P.M. Sheridan, M.J. Dick, and P.F. Bernath, J. Mol. Spectrosc. **240**, 26–31 (2006).

[11] Debayan Mitra, Nathaniel B. Vilas, Christian Hallas, Loïc Anderegg, Benjamin L. Augenbraun, Louis Baum, Calder Miller, Shivam Raval, and John M. Doyle, "Direct laser cooling of a symmetric top molecule," Science **369**, 1366–1369 (2020), https://science.sciencemag.org/content/369/6509/1366.full.pdf.

[12] John P. Perdew, Matthias Ernzerhof, and Kieron Burke, "Rationale for mixing exact exchange with density functional approximations," The Journal of Chemical Physics **105**, 9982–9985 (1996), https://doi.org/10.1063/1.472933.

[13] S. Grimme, J. Anthony, S. Ehrlich, and H. Krieg, "A consistent and accurate ab initio parametrization of density functional dispersion correction (DFT-D) for the 94 elements H-Pu." J. Chem. Phys. **132**, 154104 (2010).

[14] Yihan Shao, Ye Mei, Dage Sundholm, and Ville R. I. Kaila, "Benchmarking the performance of time-dependent density functional theory methods on biochromophores," Journal of Chemical Theory and Computation **16**, 587–600 (2020), pMID: 31815476, https://doi.org/10.1021/acs.jctc.9b00823.

[15] Carlo Adamo and Vincenzo Barone, "Toward reliable density functional methods without adjustable parameters: The PBE0 model," The Journal of Chemical Physics **110**, 6158–6170 (1999), https://doi.org/10.1063/1.478522.

[16] Paul J. Robinson, Xinxing Zhang, Tyrel McQueen, Kit H. Bowen, and Anastassia N. Alexandrova, "SmB_6^- cluster anion: Covalency involving *f* orbitals," The Journal of Physical Chemistry A **121**, 1849–1854 (2017), pMID: 28182423, https://doi.org/10.1021/acs.jpca.7b00247.

[17] Narbe Mardirossian and Martin Head-Gordon, "Thirty years of density functional theory in computational chemistry: an overview and extensive assessment of 200 density functionals," Molecular Physics **115**, 2315–2372 (2017), https://doi.org/10.1080/00268976.2017.1333644.

[18] Jingjing Zheng, Yan Zhao, and Donald G. Truhlar, "The DBH24/08 database and its use to assess electronic structure model chemistries for chemical reaction barrier heights," Journal of Chemical Theory and Computation **5**, 808–821 (2009), pMID: 26609587, https://doi.org/10.1021/ct800568m.

[19] Alessandro Ferretti, Marco d'Ischia, and Giacomo Prampolini, "Benchmarking cation-π interactions: Assessment of density functional theory and möller-plesset second-order perturbation theory calculations with optimized basis sets ($_{\mathrm{MP}}2^{\mathrm{mod}}$) for complexes of benzene, phenol, and catechol with Na^+, K^+, Rb^+, and Cs^+," The Journal of Physical Chemistry A **124**, 3445–3459 (2020), pMID: 32271571, https://doi.org/10.1021/acs.jpca.0c02090.

[20] Demeter Tzeli, Ioannis D. Petsalakis, and Giannoula Theodorakopoulos, "Molecular logic gates based on benzo-18-crown-6 ether of styrylquinoline: a theoretical study," Phys. Chem. Chem. Phys. **18**, 32132–32145 (2016).

[21] Athanasios Koliogiorgos, Christos S. Garoufalis, Iosif Galanakis, and Sotirios Baskoutas, "Electronic and optical properties of ultrasmall ABX_3 (A = Cs, CH_3NH_3/B = Ge, Pb, Sn, Ca, Sr/X = Cl, Br, I) perovskite quantum dots," ACS Omega **3**, 18917–18924 (2018), https://doi.org/10.1021/acsomega.8b02525.

[22] Dmitrij Rappoport and Filipp. Furche, "Property-optimized gaussian basis sets for molecular response calculations." J. Chem. Phys. **133**, 134105–1–134105–11 (2010).

[23] Maxim V. Ivanov, Felix H. Bangerter, and Anna I. Krylov, "Towards a rational design of laser-coolable molecules: insights from equation-of-motion coupled-cluster calculations," Phys. Chem. Chem. Phys. **21**, 19447 (2019).

[24] Maxim V. Ivanov, Felix H. Bangerter, Paweł Wójcik, and Anna I. Krylov, "Toward ultracold organic chemistry: Prospects of laser cooling large organic molecules," The Journal of Physical Chemistry Letters **11**, 6670–6676 (2020), pMID: 32787222, https://doi.org/10.1021/acs.jpclett.0c01960.

[25] C.R Brazier and P.F Bernath, "Laser and fourier transform spectroscopy of the $\tilde{A}\,^2\Pi - \tilde{X}\,^2\Sigma^+$ transition of SrOH," J. Mol. Spec. **114**, 163–173 (1985).

[26] I. Kozyryev, T. C. Steimle, P. Yu, D.-T. Nguyen, and J. M. Doyle, "Determination of CaOH and $CaOCH_3$ vibrational branching ratios for direct laser cooling and trapping," New J. Phys. **21** (2019).

[27] Anam C. Paul, Ketan Sharma, Md Asmaul Reza, Hamzeh Telfah, Terry A. Miller, and Jinjun Liu, "Laser-induced fluorescence and dispersed-fluorescence spectroscopy of the $\tilde{A}\,^2E - \tilde{X}\,^2A_1$ transition of jet-cooled calcium methoxide (CaOCH3) radicals," J. Chem. Phys. **151**, 134303 (2019).

[28] B. L. Augenbraun, J. M. Doyle, T. Zelevinsky, and I. Kozyryev, "Molecular asymmetry and optical cycling: Laser cooling asymmetric top molecules," Phys. Rev. X **10** (2020), 10.1103/physrevx.10.031022.

[29] Takatoshi Ichino, Jürgen Gauss, and John F. Stanton, "Quasidiabatic states described by coupled-cluster theory," J. Chem. Phys. **130**, 174105 (2009).

[30] Jinjun Liu, Dmitry Melnik, and Terry A. Miller, "Rotationally resolved $\tilde{B} \leftarrow \tilde{X}$ electronic spectra of the isopropoxy radical: A comparative study," J. Chem. Phys. **139**, 094308 (2013).

[31] Jinjun Liu and Terry A. Miller, "Jet-cooled laser-induced fluorescence spectroscopy of cyclohexoxy: Rotational and fine structure of molecules in nearly degenerate electronic states," J. Phys. Chem. A **118**, 11871–11890 (2014).

[32] G. Fischer, *Vibronic Coupling: The Interaction between the Electronic and Nuclear Motions* (Academic Press, 1984).

[33] Mingguang Li and John A. Coxon, "The CaCCH $\tilde{A}\,^2\Pi - \tilde{X}\,^2\Sigma^+$ 5_2^2 and 5_2^0 Bands Studied by High Resolution Spectroscopy: The Ca-C-C Bending Vibration and Vibronic Interaction," J. Mol. Spec. **183**, 250–262 (1997).

[34] P. I. Presunka and J. A. Coxon, "Laser spectroscopy of the $\tilde{A}\,^2\Pi - \tilde{X}\,^2\Sigma^+$ transition of SrOH: Deperturbation analysis of K-resonance in the $v_2 = 1$ level of the $\tilde{A}\,^2\Pi$ state," J. Chem. Phys. **101**, 201–222 (1994).

[35] Ephriem Tadesse Mengesha, Anh T. Le, Timothy C. Steimle, Lan Cheng, Chaoqun Zhang, Benjamin L. Augenbraun, Zack Lasner, and John Doyle, "Branching ratios, radiative lifetimes and transition dipole moments for YbOH," (2020), arXiv:2002.05849 [physics.atom-ph].

[36] A.V. Luzanov, A.A. Sukhorukov, and V.E. Umanskii, "Application of transition density matrix for analysis of excited states," Theor. Exp. Chem. **10**, 354 (1976).

[37] M. Head-Gordon, A.M. Grana, D. Maurice, and C.A. White, "Analysis of electronic transitions as the difference of electron attachment and detachment densities," J. Phys. Chem. **99**, 14261 (1995).

[38] Corwin Hansch, A. Leo, and R. W. Taft, "A survey of hammett substituent constants and resonance and field parameters," Chemical Reviews **91**, 165–195 (1991), https://doi.org/10.1021/cr00002a004.